Hindawi
International Journal of Energy Research
Volume 2023, Article ID 8525437, 12 pages
https://doi.org/10.1155/2023/8525437

Research Article

Investigation of Properties of Polyimide-Grafted Erythritol Composites Filled with Oxidized Expanded Graphite by *In Situ* Fabrication for Advanced Phase Change Materials

Wondu Lee and Jooheon Kim

School of Chemical Engineering and Materials Science, Chung-Ang University, Seoul 156-756, Republic of Korea

Correspondence should be addressed to Jooheon Kim; jooheonkim@cau.ac.kr

Received 5 April 2023; Revised 15 May 2023; Accepted 1 September 2023; Published 20 September 2023

Academic Editor: Nagaraj Nandihalli

Owing to their high latent heat enabling thermal energy conservation upon heat absorption and release, phase change materials (PCMs) are attracting increasing interest for use in thermal energy storage systems and next-generation thermal management systems. However, they have limitations such as inherently poor thermal and mechanical properties, which hinder their practical use. To overcome these limitations, we prepared a novel PCM based on polyimide- (PI-) grafted erythritol (PIET) through *in situ* grafting and imidization using PI. PIET composites that were prepared using oxidized expanded graphite as a filler showed an improved thermal conductivity of 2.56 $W \cdot m^{-1} \cdot K^{-1}$ in the through-plane direction, a latent heat of 192.5 $J \cdot g^{-1}$, and a tensile strength enhanced by 119%. Thus, the prepared PCM composites showed the potential for the development of advanced PCMs.

1. Introduction

The rapid development of electronic devices and packaging technologies, such as electronic power modules and energy storage system, has resulted in the development of highly integrated, high-performance, and high-density devices. However, these advances have led to thermal and electrical problems, which reduce the lifetime and reliability of the electronic devices [1–3]. In particular, for the stable and safe operation of the devices, an efficient heat management system is necessary to dissipate the heat accumulated [4, 5]. Toward this end, various studies have developed thermal interface materials consisting of a polymer matrix (epoxy [6], polyvinyl alcohol [7], and polyimide (PI) [8]) and highly thermally conductive fillers (graphite [9], graphene [10], carbon nanotubes [11], alumina [12], aluminum nitride [13], boron nitride [14], copper [15], and silver [16]). Phase change materials (PCMs) such as stearic acid [17], paraffin [18], and erythritol (ET) [19] have attracted attention as novel thermal management and energy storage systems, because of their high latent heat that facilitates heat conservation during the inflow and outflow of thermal energy. However, the inherently poor thermal and mechanical properties of these materials limit their use in real products. Furthermore, heat-induced leakage issues at temperatures above the melting point of the PCMs and supercooling effects pose additional challenges to the development of advanced PCM composites [20, 21]. One of efficient strategies to prevent leakage is microencapsulation, which has the advantage of preserving the high latent heat and leakage proof properties [22, 23]. However, most reported studies of microencapsulated PCM composites showed limited low thermal conductivity. Zhang et al. used calcium carbonate, polydopamine, and n-octadecane to fabricate form-stable PCM composite. The composite had a thermal conductivity of 0.5 $W \cdot m^{-1} \cdot K^{-1}$ and a latent heat of 140 $J \cdot g^{-1}$ [24]. Meanwhile, to introduce a porous-structured filler network in the matrix by using porous expanded graphite (EG) [25] and a metal framework [26] is also useful strategy. EG is commonly used in this context because of its low cost, porous structure, ease of surface treatment, and high thermal conductivity (100–150 $W \cdot m^{-1} \cdot K^{-1}$). Huang et al. used EG, paraffin, and styrene-butadiene-

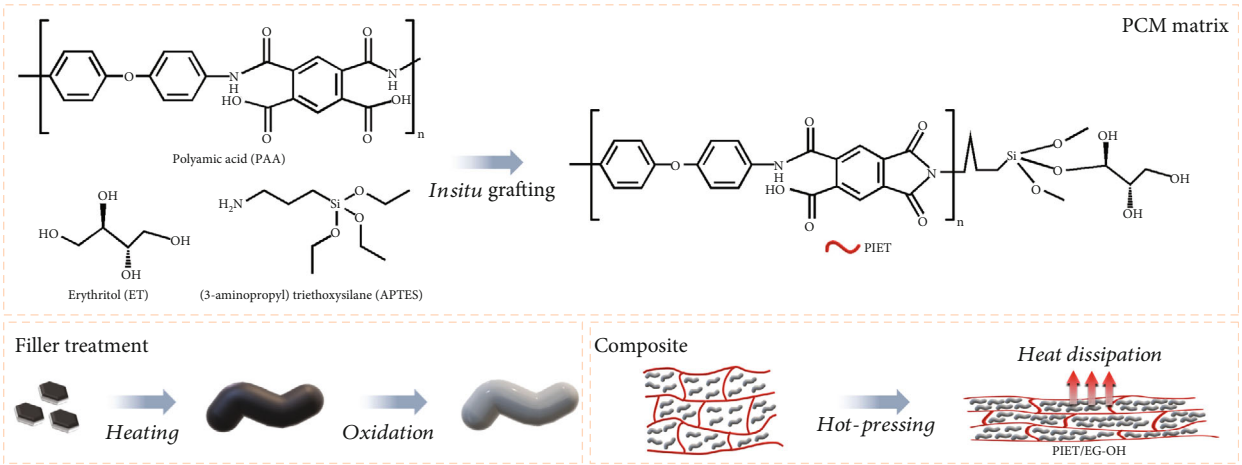

Figure 1: Fabrication process for PIET/EG-OH.

styrene to fabricate a flexible, form-stable PCM composite. The composite had a bending strength of 0.75 MPa, a tensile strength of 0.38 MPa, a thermal conductivity of 0.88 $W \cdot m^{-1} \cdot K^{-1}$, and a latent heat of 78.3 $J \cdot g^{-1}$ [27]. Moreover, ET, which is a sugar alcohol PCM, is attracting attention as a potential matrix of PCM composites, owing to its intrinsically excellent heat-saving capacity, absence of phase separation and corrosion, high thermal conductivity, and ecofriendly nature [28]. Ma et al. fabricated EG/ET PCM composites and measured their latent heat and thermal conductivity to be 352.66 $J \cdot g^{-1}$ and 1.287 $W \cdot m^{-1} \cdot K^{-1}$, respectively, which corresponded to a 52.5% improvement compared with pure ET [29]. Although improvements in thermal conductivity and mechanical properties have been reported in many studies, it is still difficult to achieve a level exceeding that of conventional polymer-matrix composites. In particular, the hot-pressing method is useful for the fabrication of high-performance composites with decreasing voids between the filler and the matrix under high pressure and at a temperature above the glass transition temperature of the polymer matrix [30, 31].

In this study, a novel PI-grafted ET (PIET) PCM was prepared through *in situ* grafting and thermal imidization using PI, ET, and (3-aminopropyl)triethoxysilane (APTES). The prepared PIET matrix showed higher mechanical and thermal stability than pure ET. Furthermore, oxidized EG (EG-OH) showed improved compatibility with the matrix, with stronger interaction and reduced thermal resistance at the interface. The prepared PIET and EG-OH were compounded using the hot-pressing method. The porous EG structure provided phonon transfer paths in the PCM and dissipated accumulated heat, thereby preventing the thermal degradation of ET. The novel PCM composite prepared in this work and its easy preparation show great potential for accelerating the development of functional PCMs.

2. Experimental Section

2.1. Materials. Meso-ET (99% purity) was supplied by Alfa Aesar, pyromellitic dianhydride-*co*-4,4′-oxydianiline poly(amic acid) (PAA) solution (electronic grade), APTES (98% purity), and expandable graphite (>300 μm) were procured from Sigma-Aldrich, and sulfuric acid and nitric acid were purchased from Daejung Chemical Co., Korea.

2.2. Synthesis of PIET. ET, PAA solution, and APTES were mixed and stirred until completely melted at 140°C for 30 min. After that, a homogeneous yellow mixture was produced. To prevent imidization, we stored the prepared PIET at room temperature.

2.3. Oxidization of EG. To synthesize porous EG, we heated expandable graphite to 900°C for 30 s in a muffle furnace. One gram of the EG synthesized was dispersed in a 450 mL mixture of sulfuric and nitric acid (1 : 2 *v*/*v*), and the mixture was stirred at 75°C for 6 h to oxidize it. After the reaction, the mixture was filtered and stored at 80°C in an oven.

2.4. Preparation of PIET/EG-OH. EG-OH was dispersed in acetone. The dispersion was then added to PIET, and the mixture was stirred at 120°C until all the acetone evaporated and the mixture was homogeneous. The mixture was taken in a Teflon plate and hot-pressed through a thermal imidization process that consisted of the following three stages.

(1) Solvent evaporation at 150°C for 10 min; only the evaporation of the solvent occurred in this stage

(2) Imidization at 230°C for 30 min

(3) Annealing at 300°C for 60 min

Finally, PIET/EG-OH composites were obtained.

3. Results and Discussion

3.1. Synthesis and Analysis of PIET. We first prepared the PIET PCM and oxidized EG to produce advanced PCM composites (Figure 1). PIET was fabricated to address the intrinsic fragility and liquid leakage issues of ET at high temperatures. This material was synthesized by imidization of PAA-ET prepared through *in situ* grafting using PI, ET, and APTES.

Fourier transform infrared (FT-IR) spectra showed the chemical reaction changes occurring in PAA-ET and PIET

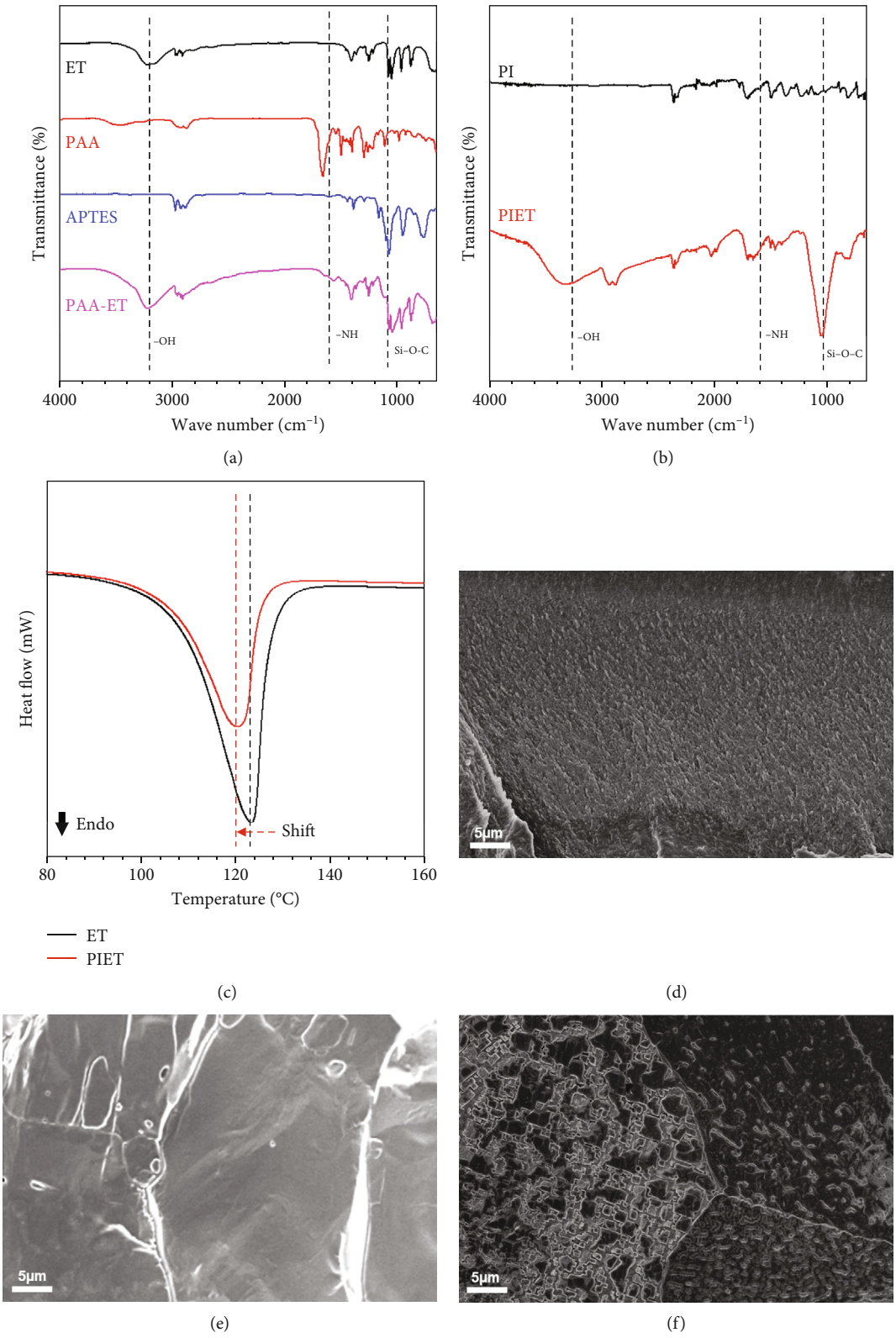

Figure 2: (a, b) FT-IR spectra and (c) DSC curve changes upon fabrication of PIET. Cross-sectional FESEM images of (d) PI, (e) neat ET, and (f) PIET are also shown.

(Figure 2(a)). The peak at 3324 cm^{-1} was attributed to the stretching vibrations of the O–H groups of ET [32], and the typical peaks at 1620 and 1098 cm^{-1} corresponded to the N–H and Si–O–C stretching vibrations of APTES [33]. After the reaction between PAA and ET, the signals of the –NH groups of APTES and PAA disappeared, and a new

Table 1: Mechanical properties and latent heat of PIET.

PI/ET ratio	Latent heat ($J \cdot g^{-1}$)	Tensile strength (MPa)	Elongation at break (%)
1 : 0 (PI)	—	70 ± 0.3	10 ± 0.2
0 : 1 (ET)	395.3 ± 0.3	0.7 ± 0.1	2.4 ± 0.1
1 : 1	191.4 ± 0.3	3.39 ± 0.2	6.37 ± 0.1
1 : 2.5	259.6 ± 0.3	2.84 ± 0.2	4.64 ± 0.1
1 : 5	328.2 ± 0.2	1.48 ± 0.2	3.79 ± 0.2

peak of Si-O-C stretching vibrations appeared, confirming the successful grafting of PAA chains on ET [34]. The broad hydroxyl vibration peak of ET also appeared after the reaction. The same results were obtained after the thermal curing of PI and PIET (Figure 2(b)).

Thermal behavior changes after the synthesis of PIET were investigated using differential scanning calorimetry (DSC). The variation in the endothermic temperature of the material is shown in Figure 2(c). The melting temperatures of PAA and ET were −20 and 130 °C, respectively. After the synthesis, the endothermic response of PIET shifted to 120–122.5°C, which was 5°C lower than that of ET. These phenomena originated from the weakening of the hydrogen bond network because of the reduction in the number of hydroxyl groups (related to the melting point of the material) during the grafting of PAA on ET. In other words, the decreased melting point of PAA-ET was a strong indication of the successful grafting of PAA on ET [35].

Cross-sectional images (Figures 2(d)–2(f)) of the matrices during the PIET synthesis were obtained using field-emission scanning electron microscopy (FE-SEM). A homogeneous PIET phase was observed after the synthesis, consistent with the above results (Figures 2(e) and 2(f)).

The mechanical properties and latent heat measured for various PI/ET ratios are shown in Table 1. Grafting PI on ET significantly enhanced the tensile strain and strength of ET due to intrinsic high mechanical properties of PI grafted on ET. Furthermore, the latent heat of the sample with PI/ET = 1 : 5 did not decrease significantly (83% of that of neat ET).

3.2. Oxidation of EG Surface and Analysis. EG was oxidized to increase the adhesion between the matrix and the filler and to thereby enhance the performance of the PCM composites.

FT-IR analysis was conducted to evaluate changes in the functional groups during the oxidation process (see Figure 3(a)). A new peak of 3325 cm^{-1}, which was attributed to the O–H vibration, was observed for EG-OH. To obtain additional information, we performed wide-scan X-ray photoelectron spectroscopy (XPS) and Raman measurements (Figures 3(b) and 3(c)). XPS analysis showed that the O/C atomic ratio increased from 0.015 (raw EG) to 0.16 (EG-OH), and the Raman spectrum of EG was dominated by the G, D, and 2D bands. The peak at 1355 cm^{-1} (D band) was attributed to defects on the surface of EG and the sp^3-hybridized carbon, the peak at 1578 cm^{-1} (G band) was the vibration of sp^2-bonded carbon atoms, and the 2718 cm^{-1} peak of the 2D band was the second order of the D band that could be attributed to two-phonon emission with double resonant Raman scattering [34]. The I_D/I_G ratio—the intensity ratio between the D and G bands—is used to evaluate the amount of disorder and defects in carbon materials [36]. The I_D/I_G ratio of EG and EG-OH increased from 0.14 to 0.21 after oxidation, reflecting an increase in defects in EG-OH because of the introduction of hydroxyl groups in the oxidation process. These results confirmed the successful introduction of hydroxyl groups on the EG surface [37].

3.3. Morphological Analysis of EG. Morphological changes that occurred during the preparation of EG-OH were analyzed using FE-SEM (Figures 3(d)–3(f)). Figure 3(d) shows the presence of expandable graphite flakes, and Figure 3(e) depicts the porous structure of EG after heating. Notably, the porous EG structure was well maintained after oxidation (Figure 3(f)).

3.4. Morphology of PIET/EG-OH Composites. The stronger interfacial interaction between EG-OH and the matrix after oxidation was verified by performing FE-SEM morphological analysis (Figure 4).

Raw EG exhibited many defects and a low dispersibility, which resulted in the separation of the matrix and filler domains because of poor interfacial interaction (Figures 4(a) and 4(c)). On the other hand, EG-OH showed significantly enhanced interfacial adhesion in the PIET, owing to the hydrogen bonds between ET's hydroxyl groups and the filler surface (Figures 4(b) and 4(d)).

3.5. Properties. The through-plane thermal conductivity was calculated by measuring the thermal diffusivity, heat capacity, and density of PIET composites according to various constitutions (Figure 5(a)). As expected, PIET/EG-OH exhibited the highest thermal conductivity (2.56 $W \cdot m^{-1} \cdot K^{-1}$, 412% higher than that of pure ET (0.5 $W \cdot m^{-1} \cdot K^{-1}$)). In other words, the improvement in the interfacial interaction after the oxidation of EG, the porous filler network of EG in the through-plane direction, and the reduction in the number of defects in composites fabricated through hot-pressing resulted in the prepared PCMs having high thermal conductivity. Additionally, a theoretical analysis was conducted to predict the thermal conductivity of composites for analyzing the increasing trend of the thermal conductivity of composites in detail, and it is described in the extended discussion part in Supplementary Information (Figure S1 and Table S1).

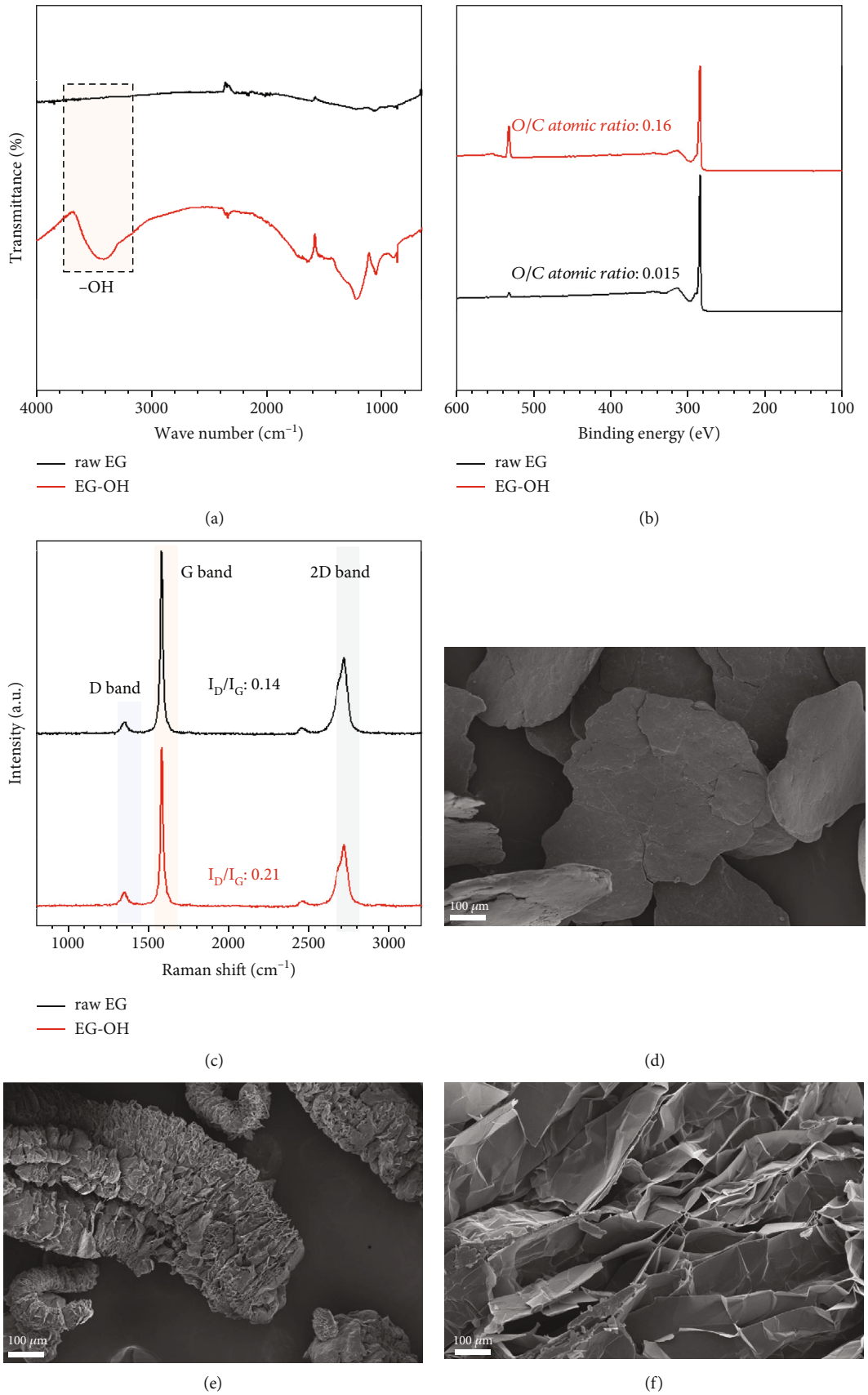

Figure 3: (a) FT-IR, (b) wide-scan XPS, and (c) Raman spectra of EG and EG-OH. Morphologies of (d) EG flakes, (e) EG, and (f) EG-OH.

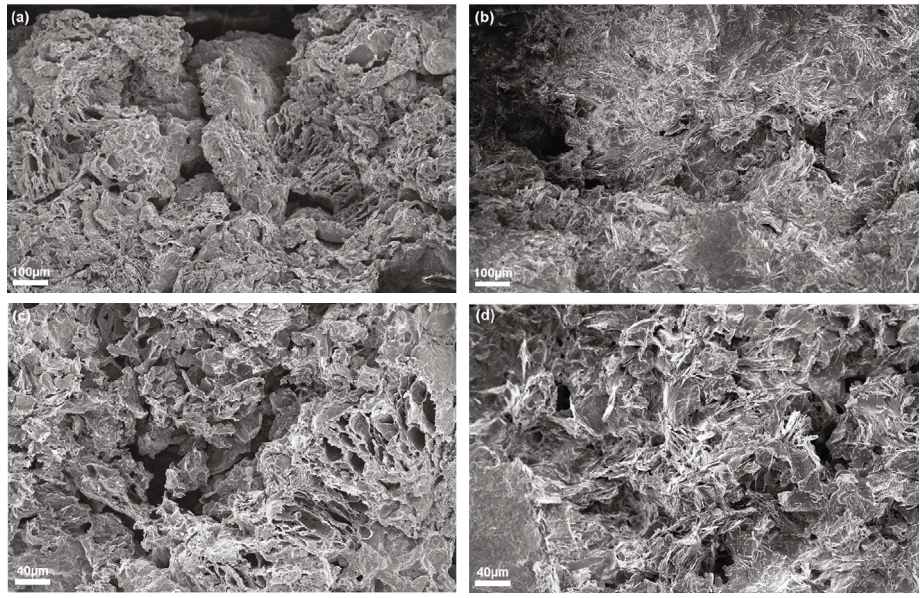

Figure 4: Cross-sectional FE-SEM images of (a, c) PIET/EG and (b, d) PIET/EG-OH.

Figure 5(c) shows the latent heat values measured for PCMs with different fillers. The latent heat of PIET/raw EG was only 51.2% (168.2 J·g^{-1}) of that of PIET (328.2 J·g^{-1}), and this could be ascribed to the crystal orientation of ET molecules being constrained by the porous EG [38]. The steric drag effect of nano is also known to decrease the latent heat of form-stable PCMs [39]. After the oxidation of EG, improved interfacial interaction resulting from hydrogen bonding between hydroxyl groups on the EG surface and the ET matrix accelerated heat transfer in the PIET/EG-OH composite. Consequently, PIET/EG-OH had higher latent heat (192.5 J·g^{-1}, enhancement of approximately 14%) than PIET/raw EG.

To verify the superiority of the PIET/EG-OH composites, we compared the dependence of their thermal conductivity on the latent heat with that in the case of sugar alcohol-based PCM composites reported in recent studies (Table 2). Since it is difficult to simultaneously achieve high values of latent heat and thermal conductivity, PIET/EG-OH (with high latent heat and thermal conductivity) has high potential for use in novel thermal management applications combining heat dissipation and saving.

Furthermore, the thermal stability of PIET/EG-OH was evaluated via a leakage test. As shown in Figure 6, pure ET start to leak at 150°C while PIET start to leak at 170°C. This is due to cured PI between ET that enhance the thermal stability of PIET. Meanwhile, PIET/EG-OH did not show any leakage of ET up to 200°C, which is considerably higher than the melting point of ET (130°C). In other words, the chemical curing reaction between PI and ET, the porous EG network, and the hydrogen interaction between interfaces of filler and matrix significantly enhanced the thermal stability of the composites.

The tensile stress and strain of PIET/EG-OH were evaluated by using a universal testing machine (Figures 7(a) and 7(b)). After raw EG was loaded, the tensile strain and stress increased from 3.79% to 4.28% and from 1.48 MPa to 1.99 MPa, respectively, because of the brittleness of the filler [45]. Furthermore, the EG-OH filler network and the improved interfacial interaction between the filler and the matrix maintained the tensile strain at 5.09%, which caused the tensile strength to increase to 2.59 MPa. The tensile strength and stress increased by 119% and 225%, respectively, compared with those of pure ET. Thus, among reported PCM composites, the PIET/EG-OH composite is a strong candidate for use as an advanced PCM.

Figure 8 and Table 3 show a comparison between the cooling curves and subcooling degrees of the PCM composites. When a material passes through a metastable phase transition temperature during the cooling or heating process without solidifying or melting, subcooling occurs. This is considered a kinetic property, and the difference between the melting temperature (T_m) and the solidification temperature (T_s) is the subcooling degree (T_{sc}). Most PCMs used in thermal storage applications exhibit subcooling, and this property is less pronounced in organic PCMs such as paraffins and fatty acids compared with inorganic PCMs such as salt hydrates. To verify the subcooling impact of composites with various components, we determined the subcooling degree by using DSC. For neat ET, the subcooling degree was 68.7°C, which is a large value typical of sugar alcohol-based PCMs. The porous EG with a large specific area can influence the ET matrix in two ways. First, it can increase the nucleation sites in ET and promote nucleation and crystal growth. Second, the porous structure can adsorb and fix ET, which would hinder the diffusion of ET molecules and improve the activation energy of phase transformation. From Figure 8 and Table 3, the supercooling degree after EG loading (44.8) was apparently lower than that of pure ET, implying that the nucleation effect of EG was stronger than the hindrance effect. Furthermore, the improved interfacial interaction between ET and EG-OH after the oxidation of the EG surface enhanced the nucleation effect and decreased the supercooling degree of the PIET/EG-OH composite (39) [50]. Meanwhile, the phase change stability of

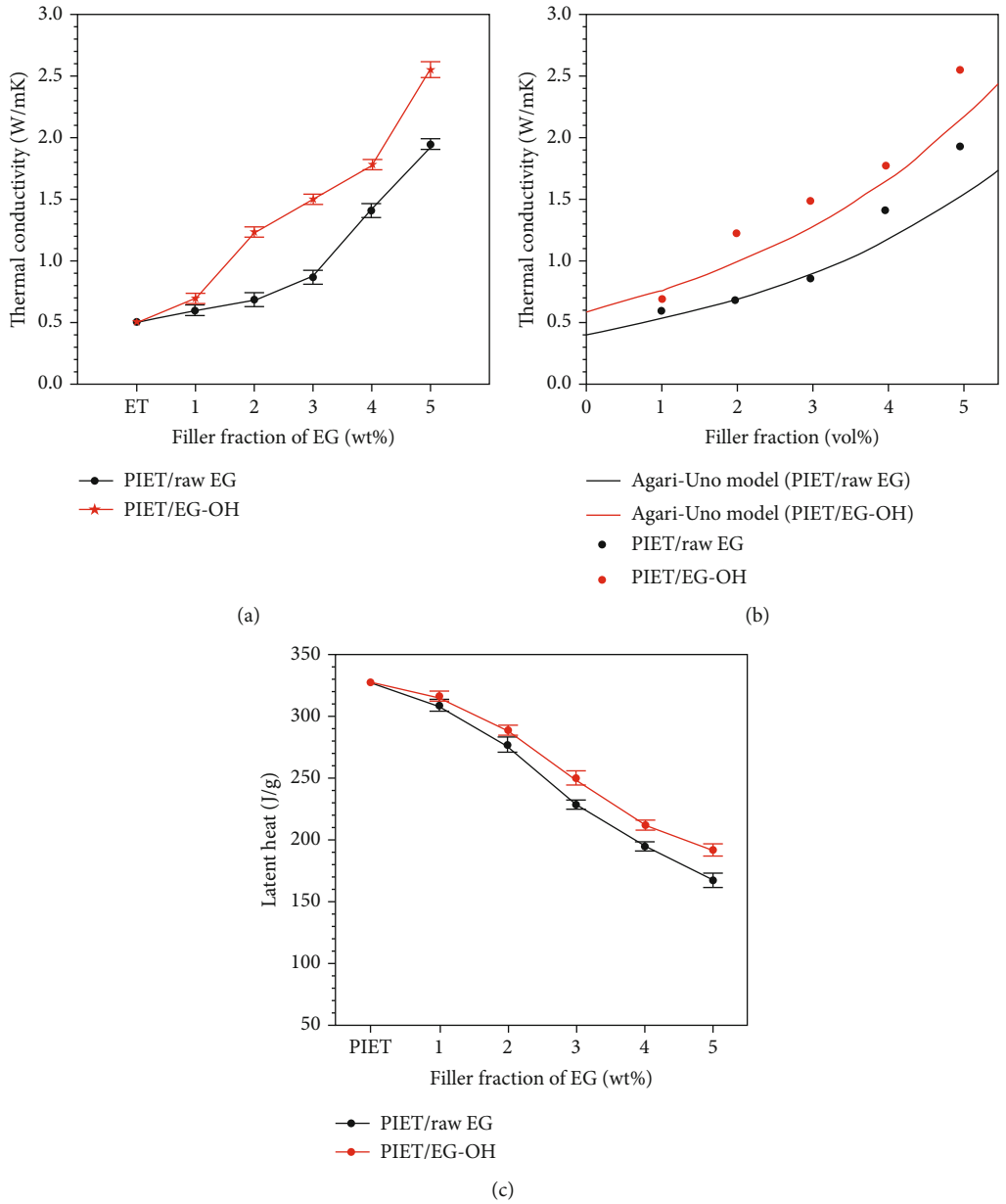

Figure 5: (a) Through-plane thermal conductivity, (b) modeling (Agari-Uno model) of composites, and (c) latent heat of PIET composites.

Table 2: Comparison of thermal properties of sugar alcohol-based PCM composites.

Organic PCMs	Filler	Filler content (%)	Latent heat ($J \cdot g^{-1}$)	Thermal conductivity ($W \cdot m^{-1} \cdot K^{-1}$)	Refs.
56ME/Sep	xGNP	8	168.9	0.76	[38]
Erythritol	KKf	7	322.5	0.40	[40]
D-Mannitol	Silica/GO	—	216.7	0.72	[41]
Erythritol	EG/CaPi	3	352.7	1.29	[42]
Erythritol	MWCNT	1	356.0	0.98	[43]
Erythritol	Exfoliated graphite	10	257.5	1.66	[44]
Erythritol	EG	4	380.5	1.15	[46]
PIET	EG-OH	5	192.5	2.56	The present work

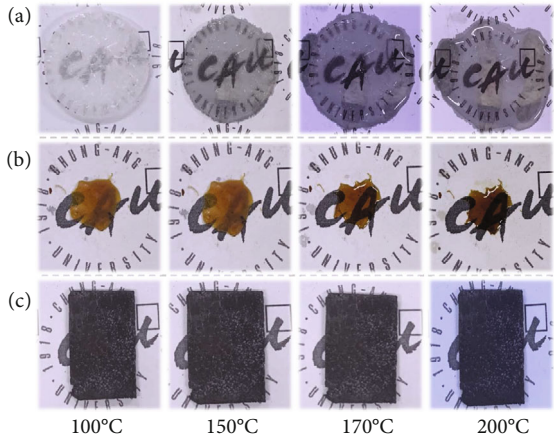

Figure 6: Leakage test at different temperatures for (a) neat ET, (b) PIET (PI/ET ratio = 1 : 5), and (c) PIET/EG-OH.

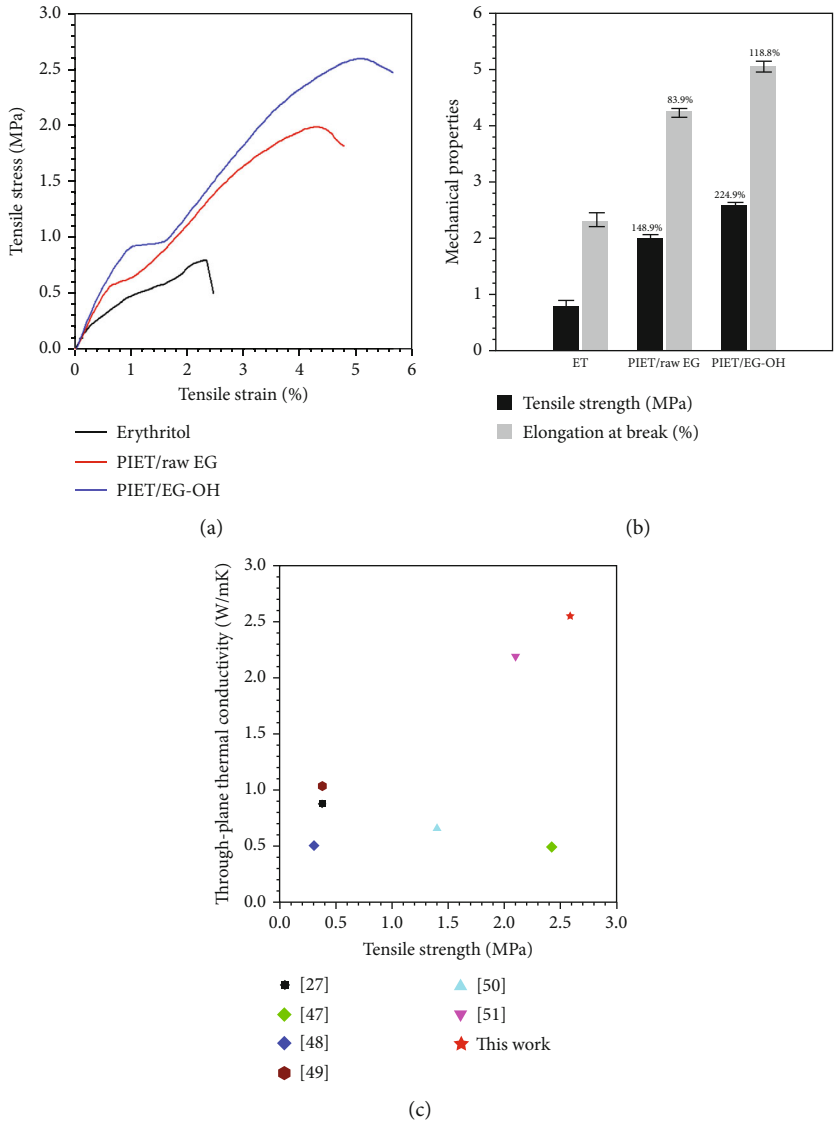

Figure 7: Mechanical properties of PIET composites (a, b). Comparison of thermal conductivity according to tensile strength of reported PCM composites (c) [27, 47–51].

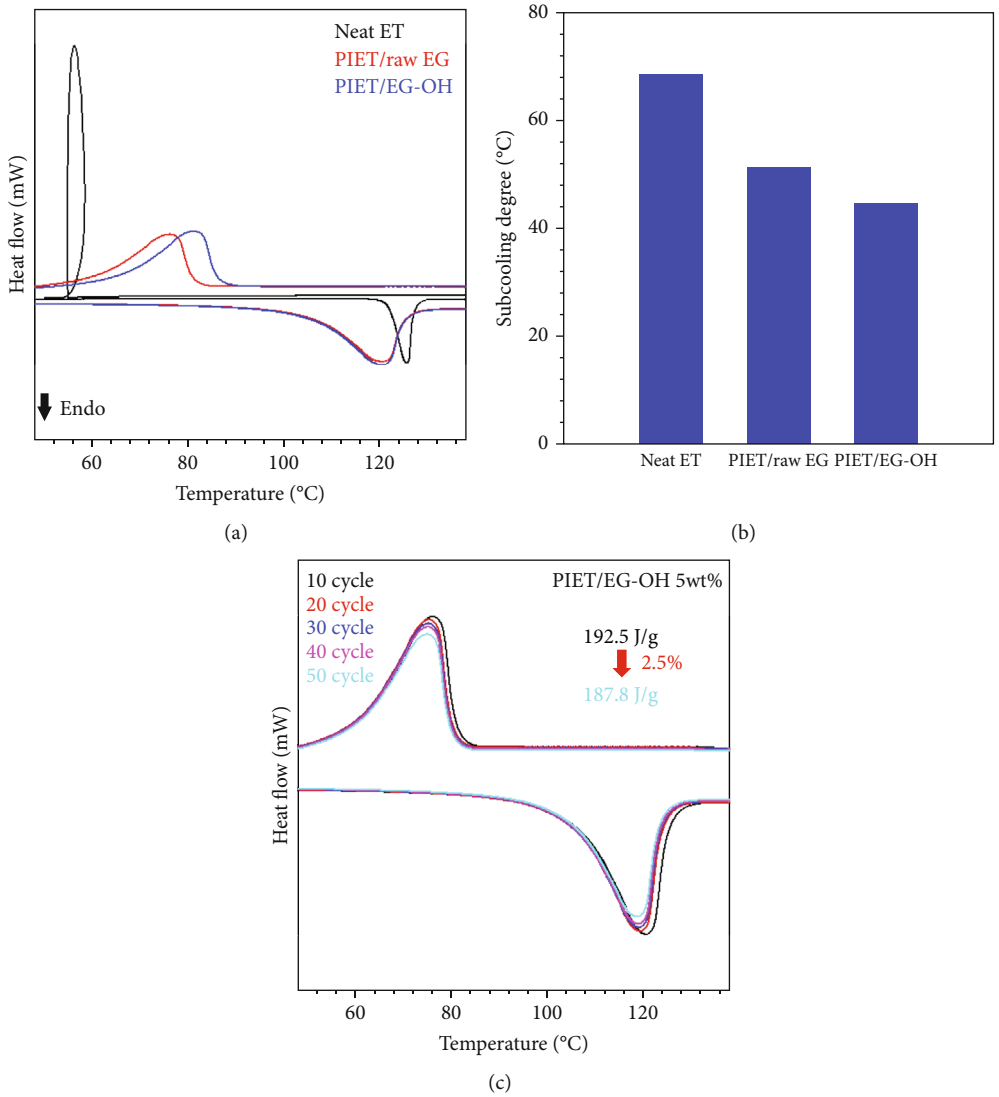

Figure 8: (a) DSC curves and (b) subcooling degree of composites. (c) DSC cycling test of PIET/EG-OH.

Table 3: Subcooling degree of composites with different components.

Composite	Melting temperature (°C)	Solidifying temperature (°C)	Subcooling degree (°C)
Neat ET	125.8 ± 0.1	57.1 ± 0.2	68.7
PIET/raw EG	120.2 ± 0.2	75.4 ± 0.1	44.8
PIET/EG-OH	120.3 ± 0.1	81.3 ± 0.1	39

PCM composites is also one of the most critical factors. Therefore, DSC cycling tests with 50 cycles were performed to confirm the decrease in the latent heat during repeating phase changes (Figure 8(c)). After 50 cycles, the latent heat of the composites decreased from 192.5 to 182.8 $J \cdot g^{-1}$ (i.e., only by 2.5%), indicating that the phase change stability in repeating heating and cooling cycles is sufficient.

4. Conclusions

We attempted to fabricate novel thermal conductive PCMs that did not have the drawbacks of existing PCMs, such as poor mechanical properties and low thermal conductivity. The novel PCMs were synthesized through *in situ* grafting using PI, ET, and APTES. To increase the interfacial adhesion between the matrix and the filler, we oxidized the EG surface. The fabricated PIET/EG-OH composites showed excellent characteristics such as high through-plane thermal conductivity (2.56 $W \cdot m^{-1} \cdot K^{-1}$), tensile strength (2.59 MPa), and latent heat (192.5 $J \cdot g^{-1}$). Our study shows the considerable potential of thermal conductive PCM composites for novel thermal management applications, including heat saving and heat dissipation, which will significantly contribute to the further development of these composites.

Data Availability

All data generated or analyzed during this study are included in this paper. Raw datasets are available from the corresponding author on reasonable request.

Conflicts of Interest

The authors declare that they have no conflicts of interest.

Acknowledgments

This work was supported by the Industrial Technology Innovation Program (20019205) funded by the Ministry of Trade, Industry & Energy (MOTIE, Korea) and also supported by the National Research Foundation of Korea (NRF) grant funded by the Korea government (MSIT) (NRF-2022M3H4A1A02076956).

Supplementary Materials

Characterization and extended discussions. *(Supplementary Materials)*

References

[1] Y. Yang, L. Dorn-Gomba, R. Rodriguez, C. Mak, and A. Emadi, "Automotive power module packaging: current status and future trends," *IEEE Access*, vol. 8, pp. 160126–160144, 2020.

[2] G. Moreno, S. Narumanchi, X. Feng, P. Anschel, S. Myers, and P. Keller, "Electric-drive vehicle power electronics thermal management: current status, challenges, and future directions," *Journal of Electronic Packaging*, vol. 144, no. 1, 2022.

[3] C.-C. Lee, K.-S. Kao, C.-W. Wang, T.-J. Yu, T.-K. Lee, and P.-K. Chiu, "Assembly reliability and molding material comparison of miniature integrated high power module with insulated metal substrate," *Journal of Electronic Packaging*, vol. 144, no. 2, 2022.

[4] M. Maqbool, W. Aftab, A. Bashir, A. Usman, H. Guo, and S. Bai, "Engineering of polymer-based materials for thermal management solutions," *Composites Communications*, vol. 29, article 101048, 2022.

[5] J. Lin, X. Liu, S. Li, C. Zhang, and S. Yang, "A review on recent progress, challenges and perspective of battery thermal management system," *International Journal of Heat and Mass Transfer*, vol. 167, article 120834, 2021.

[6] J. Luo, X. Yang, R. Tusiime et al., "Synergistic effect of multiscale BNs/CNT and 3D melamine foam on the thermal conductive of epoxy resin," *Composites Communications*, vol. 29, article 101044, 2022.

[7] F. Luo, M. Zhang, S. Chen, J. Xu, C. Ma, and G. Chen, "Sandwich-structured PVA/rGO films from self-construction with high thermal conductivity and electrical insulation," *Composites Science and Technology*, vol. 207, article 108707, 2021.

[8] W. Chen, W. Chen, B. Zhang, S. Yang, and C.-Y. Liu, "Thermal imidization process of polyimide film: interplay between solvent evaporation and imidization," *Polymer*, vol. 109, pp. 205–215, 2017.

[9] X. Wu, B. Tang, J. Chen et al., "Epoxy composites with high cross-plane thermal conductivity by constructing all-carbon multidimensional carbon fiber/graphite networks," *Composites Science and Technology*, vol. 203, article 108610, 2021.

[10] J. Gao, Q. Yan, L. Lv et al., "Lightweight thermal interface materials based on hierarchically structured graphene paper with superior through-plane thermal conductivity," *Chemical Engineering Journal*, vol. 419, article 129609, 2021.

[11] A. W. Kuziel, G. Dzido, R. Turczyn et al., "Ultra-long carbon nanotube-paraffin composites of record thermal conductivity and high phase change enthalpy among paraffin-based heat storage materials," *Journal of Energy Storage*, vol. 36, article 102396, 2021.

[12] Z. Wei, X. Kong, J. Cheng, H. Zhou, J. Yu, and S. Lu, "Constructing a "pearl-necklace-like" architecture for enhancing thermal conductivity of composite films by electrospinning," *Composites Communications*, vol. 29, article 101036, 2022.

[13] M. S. B. Hoque, Y. R. Koh, J. L. Braun et al., "High in-plane thermal conductivity of aluminum nitride thin films," *ACS Nano*, vol. 15, no. 6, pp. 9588–9599, 2021.

[14] Y. Zhang, H. He, B. Huang, S. Wang, and X. He, "Enhanced thermal conductivity of polyvinyl alcohol insulation composites with m-BN@CNW hybrid materials," *Composites Science and Technology*, vol. 208, article 108766, 2021.

[15] D. Liu, J. Zhao, Y. Ning et al., "Constructing zebra skin structured graphene/copper composites with ultrahigh thermal conductivity," *Composites Communications*, vol. 25, article 100704, 2021.

[16] Z. Zhang, X. Fu, H. Yu et al., "Enhanced the thermal conductivity of hydroxyl-terminated polybutadiene (HTPB) composites by graphene-silver hybrid," *Composites Communications*, vol. 24, article 100661, 2021.

[17] W. Jin, L. Jiang, L. Chen et al., "Enhancement of thermal conductivity by graphene as additive in lauric-stearic acid/treated diatomite composite phase change materials for heat storage in building envelope," *Energy and Buildings*, vol. 246, article 111087, 2021.

[18] Y. Zhou, S. Li, Y. Zhao, Z. Ling, Z. Zhang, and X. Fang, "Compatible paraffin@SiO_2 microcapsules/polydimethylsiloxane composites with heat storage capacity and enhanced thermal conductivity for thermal management," *Composites Science and Technology*, vol. 218, article 109192, 2022.

[19] M. Yuan, C. Xu, T. Wang, T. Zhang, X. Pan, and F. Ye, "Supercooling suppression and crystallization behaviour of erythritol/expanded graphite as form-stable phase change material," *Chemical Engineering Journal*, vol. 413, article 127394, 2021.

[20] X. Jin, Q. Xiao, T. Xu et al., "Thermal conductivity enhancement of a sodium acetate trihydrate-potassium chloride-urea/expanded graphite composite phase-change material for latent heat thermal energy storage," *Energy and Buildings*, vol. 231, article 110615, 2021.

[21] H. Zhang, L. Wang, S. Xi, H. Xie, and W. Yu, "3D porous copper foam-based shape-stabilized composite phase change materials for high photothermal conversion, thermal conductivity and storage," *Renewable Energy*, vol. 175, pp. 307–317, 2021.

[22] A. Subasi, S. Subasi, M. Bayram et al., "Effect of carbon nanotube and microencapsulated phase change material utilization on the thermal energy storage performance in UV cured (photoinitiated) unsaturated polyester composites," *Journal of Energy Storage*, vol. 61, article 106780, 2023.

[23] A. Can, "Preparation, characterization, and thermal properties of microencapsulated palmitic acid with ethyl cellulose shell as phase change material impregnated wood," *Journal of Energy Storage*, vol. 66, article 107382, 2023.

[24] X. Zhang, Y. Zhang, H. Li, and Z. Chen, "Enhanced thermal conductivity and photothermal effect of microencapsulated n-octadecane phase change material with calcium carbonate-polydopamine hierarchical shell for solar energy storage," *Solar Energy Materials & Solar Cells*, vol. 256, article 112336, 2023.

[25] D. Bao, Y. Gao, Y. Cui et al., "A novel modified expanded graphite/epoxy 3D composite with ultrahigh thermal conductivity," *Chemical Engineering Journal*, vol. 433, article 133519, 2022.

[26] A. Chibani, S. Merouani, and F. Benmoussa, "Computational analysis of the melting process of phase change material-metal foam-based latent thermal energy storage unit: the heat exchanger configuration," *Journal of Energy Storage*, vol. 42, article 103071, 2021.

[27] Q. Huang, X. Li, G. Zhang, J. Deng, and C. Wang, "Thermal management of lithium-ion battery pack through the application of flexible form-stable composite phase change materials," *Applied Thermal Engineering*, vol. 183, article 116151, 2021.

[28] X. Yan, H. Zhao, Y. Feng et al., "Excellent heat transfer and phase transformation performance of erythritol/graphene composite phase change materials," *Composites Part B: Engineering*, vol. 228, article 109435, 2022.

[29] C. Ma, J. Wang, Y. Wu, Y. Wang, Z. Ji, and S. Xie, "Characterization and thermophysical properties of erythritol/expanded graphite as phase change material for thermal energy storage," *Journal of Energy Storage*, vol. 46, article 103864, 2022.

[30] J. Kim, G. Kim, S.-Y. Kim et al., "Fabrication of highly flexible electromagnetic interference shielding polyimide carbon black composite using hot-pressing method," *Composites Part B: Engineering*, vol. 221, article 109010, 2021.

[31] D. Friedrich, "Thermoplastic moulding of wood-polymer composites (WPC): a review on physical and mechanical behaviour under hot-pressing technique," *Composite Structures*, vol. 262, article 113649, 2021.

[32] X. Qin, N. Feng, Z. Kang, and D. Hu, "Construction of wood-based cellulose micro-framework composite form-stable multifunctional materials with thermal and electrical response via incorporating erythritol-urea (thiourea)-carbon nanotubes," *International Journal of Biological Macromolecules*, vol. 184, pp. 538–550, 2021.

[33] X. Zhi, Y. Mao, Z. Yu et al., "γ-Aminopropyl triethoxysilane functionalized graphene oxide for composites with high dielectric constant and low dielectric loss," *Composites. Part A, Applied Science and Manufacturing*, vol. 76, pp. 194–202, 2015.

[34] C. Wang, B. Cong, J. Zhao et al., "In situ synthesis of MWCNT-graft-polyimides: thermal stability, mechanical property and thermal conductivity," *RSC Advances*, vol. 10, no. 23, pp. 13517–13524, 2020.

[35] J. Puig, I. E. Dell' Erba, W. F. Schroeder, C. E. Hoppe, and R. J. Williams, "Epoxy-based organogels for thermally reversible light scattering films and form-stable phase change materials," *ACS Applied Materials & Interfaces*, vol. 9, no. 12, pp. 11126–11133, 2017.

[36] M. Kasztelan, A. Słoniewska, M. Gorzkowski, A. Lewera, B. Pałys, and S. Zoladek, "Ammonia modified graphene oxide - gold nanoparticles composite as a substrate for surface enhanced Raman spectroscopy," *Applied Surface Science*, vol. 554, article 149060, 2021.

[37] Y. Liu and Y. Yang, "Form-stable phase change material based on Na2CO3·10H2O-Na2HPO4·12H2O eutectic hydrated salt/expanded graphite oxide composite: the influence of chemical structures of expanded graphite oxide," *Renewable Energy*, vol. 115, pp. 734–740, 2018.

[38] N. Tan, T. Xie, Y. Feng et al., "Preparation and characterization of erythritol/sepiolite/exfoliated graphite nanoplatelets form-stable phase change material with high thermal conductivity and suppressed supercooling," *Solar Energy Materials & Solar Cells*, vol. 217, article 110726, 2020.

[39] K. Nakano, Y. Masuda, and H. Daiguji, "Crystallization and melting behavior of erythritol in and around two-dimensional hexagonal mesoporous silica," *Journal of Physical Chemistry C*, vol. 119, no. 9, pp. 4769–4777, 2015.

[40] J. An, W. Liang, P. Mu et al., "Novel sugar alcohol/carbonized kapok fiber composites as form-stable phase-change materials with exceptionally high latent heat for thermal energy storage," *ACS Omega*, vol. 4, no. 3, pp. 4848–4855, 2019.

[41] L. He, S. Mo, P. Lin, L. Jia, Y. Chen, and Z. Cheng, "D-mannitol@silica/graphene oxide nanoencapsulated phase change material with high phase change properties and thermal reliability," *Applied Energy*, vol. 268, article 115020, 2020.

[42] J.-L. Zeng, Y.-H. Chen, L. Shu et al., "Preparation and thermal properties of exfoliated graphite/erythritol/mannitol eutectic composite as form-stable phase change material for thermal energy storage," *Solar Energy Materials & Solar Cells*, vol. 178, pp. 84–90, 2018.

[43] L. Gao, J. Zhao, Q. An, D. Zhao, F. Meng, and X. Liu, "Experiments on thermal performance of erythritol/expanded graphite in a direct contact thermal energy storage container," *Applied Thermal Engineering*, vol. 113, pp. 858–866, 2017.

[44] M. Barczewski, K. Sałasińska, and J. Szulc, "Application of sunflower husk, hazelnut shell and walnut shell as waste agricultural fillers for epoxy-based composites: a study into mechanical behavior related to structural and rheological properties," *Polymer Testing*, vol. 75, pp. 1–11, 2019.

[45] P. Cheng, H. Gao, X. Chen et al., "Flexible monolithic phase change material based on carbon nanotubes/chitosan/poly(vinyl alcohol)," *Chemical Engineering Journal*, vol. 397, article 125330, 2020.

[46] Q. Huang, J. Deng, X. Li, G. Zhang, and F. Xu, "Experimental investigation on thermally induced aluminum nitride based flexible composite phase change material for battery thermal management," *Journal of Energy Storage*, vol. 32, article 101755, 2020.

[47] Y. Guo, W. Yang, Z. Jiang et al., "Silicone rubber/paraffin@silicon dioxide form-stable phase change materials with thermal energy storage and enhanced mechanical property," *Solar Energy Materials & Solar Cells*, vol. 196, pp. 16–24, 2019.

[48] Z. Ding, W. Yang, F. He et al., "GO modified EPDM/paraffin shape-stabilized phase change materials with high elasticity and low leakage rate," *Polymer*, vol. 204, article 122824, 2020.

[49] Z. Cai, J. Liu, Y. Zhou et al., "Flexible phase change materials with enhanced tensile strength, thermal conductivity and photo-thermal performance," *Solar Energy Materials & Solar Cells*, vol. 219, article 110728, 2021.

[50] S. Shen, S. Tan, S. Wu et al., "The effects of modified carbon nanotubes on the thermal properties of erythritol as phase change materials," *Energy Conversion and Management*, vol. 157, pp. 41–48, 2018.

[51] F. Nazeer, Z. Ma, L. Gao, F. Wang, M. A. Khan, and A. Malik, "Thermal and mechanical properties of copper-graphite and copper-reduced graphene oxide composites," *Composites Part B: Engineering*, vol. 163, pp. 77–85, 2019.